EGF SIMULATION OF HIGH FREQUENCY GROUND MOTION. A CASE STUDY FOR M_w=5.0 CENTRAL MARMARA FAULT EARTHQUAKE

A.Mert
Boğaziçi University, Kandilli Observatory and Earthquake Research Institute, Cengelkoy, Istanbul

Y. Fahjan
Gebze Institute of Technology, Çayırova, Gebze

A.Pınar
Istanbul University, Faculty of Engineering, Avcılar, Istanbul

L. Hutchings
Lawrence Berkeley National Laboratory, 1 Cyclotron Road, 900425 Berkeley, California

SUMMARY
This study aim to simulate midsize earthquake (M_w=5.0) recorded on the northwestern portion of North Anatolian Fault Zone in Marmara Sea. Computations of realistic time histories for different locations around Marmara region would be a big contribution for earthquake hazard studies. Several researchers tried to model high frequency ground motions in Marmara Region using stochastic simulation technique depends on calculated velocity structure model. Because Marmara Region has geological complexities and heterogenic crustal structure that kind of velocity model can be produced unrealistic results. The empirical Green's function (EGF) method is one of the simplest techniques for predicting ground motion including geological heterogeneity effects. We used ground motion simulation algorithm based on EGF developed by Hutchings and Wu (1990) to obtain three dimensional time history for five different broadband stations. Similarities between recorded and simulated traces reveal that EGF method successfully represent geological heterogeneity in Marmara region.

Keywords: Earthquake simulation, Empirical Green's functions, North Anatolian fault zone, Marmara sea

1. INTRODUCTION

The Marmara Region is situated Northwestern Turkey and covers Marmara Sea Basin and surrounding areas (Figure 1). Considering the distributions of the earthquake epicenters together with the results of bathymetric and seismic studies, the active tectonics of the Marmara Sea are primarily controlled by the North Anatolian Fault Zone (NAFZ) (Gökaşan et al., 2003; Şengör et al., 2005; Yılmaz et al., 2009). Tectonically Marmara Region has a complex and heterogeneous fault system (Barka and Kandinsky-Cade, 1988) together with high seismic activity (Figure 1). Due to complex tectonic and geological structure, the western part of the NAFZ shows strong lateral heterogeneity (Barış et al., 2005). In consistent way laterally varying tomographic velocity model (Karabulut, 2003) and inhomogeneous sharp velocity variations clearly reflects geological complexities and heterogenic crustal structure in Marmara Region (Barış et al 2005).

During the past century, there has been a westward migration of large, destructive earthquakes along the NAFZ. Ruptures result from 1999 İzmit and Gölcük earthquakes represent the last chain of the succession of large earthquakes along the Northern branch of NAFZ (Toksöz et al. 1999) in the eastern part of the Marmara Sea. Other major event occurred immediately to the west of the sea in 1912 along the Northern branch of the NAFZ. These catastrophic earthquakes that occurred during the last century in the Marmara Region constitute an agreement in the scientific community that whole submarine section of the northern branch of NAFZ between 1912 and 1999 earthquake rupture can be

define as a seismic gap (Pinar 2003). According to Parson *et al.* (2004), the probability of a M ≥ 7 earthquake rupturing beneath the Sea of Marmara is 35–70% in the next 30 years if a time-dependent model that includes co-seismic and post-seismic effects of the 1999 M = 7.4 Izmit earthquake is used.

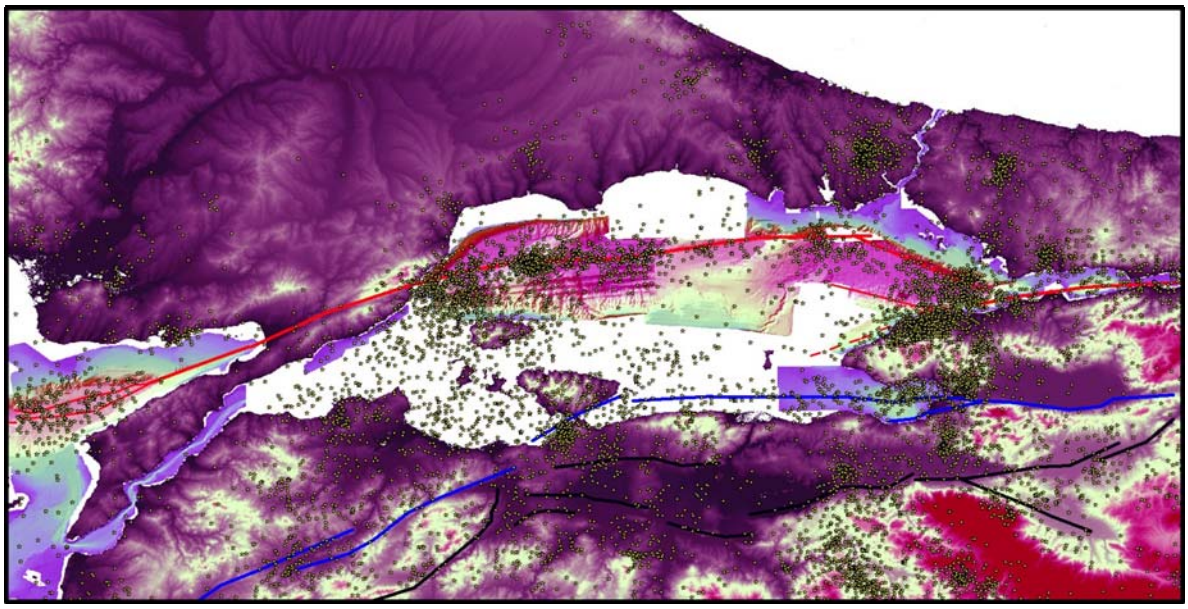

Figure 1. The branches of NAFZ in the Marmara Region. Segmentation compiled from Barka and Kadinsky-Cade (1988), Armijo et al. (2002), Yılmaz et al. (2009). The red, blue and black lines correspond to the northern, middle and southern branches of the NAFZ respectively. The yellow stars shows M_l>2 earthquake from 1999 to 2011 in the region based on BU-KOERI database.

Because of the increasing awareness of earthquake threat in the Marmara Region, the need for seismic hazard studies has become progressively more important for planning risk reduction actions. Earthquake hazard in the Marmara Region has been studied by probabilistic methods (Atakan et al., 2002; Erdik et al., 2004). Together with these earthquake hazard assessment studies, some researchers tried to model the bedrock ground motions in the Marmara Region using Hybrid broadband simulation technique (Pulido et al., 2004; Mathilde et al., 2007; Ansal et al., 2008). Pulido et al., (2004) combined deterministic simulation of seismic wave propagation at low frequencies with a semi-stochastic procedure for the high frequencies to model bedrock broadband ground motion in the Marmara region. Mathilde et al., (2007) also used the same hybrid model, semi-stochastic procedure for the high frequency and deterministic model for the low frequency, to evaluate the influence of source and attenuation parameters on the simulated ground motion. Ansal et al., (2008) to develop earthquake loss scenarios in terms of building damage and casualties for Istanbul computed synthetic time series of ground motion using by hybrid stochastic-deterministic approach.

Recently, increasing the knowledge of NAFZ within the Marmara Sea and recording huge amount of broadband seismometer and accelerometer data within the region, promote high frequency simulations of ground motion for Marmara region based on empirical Green's functions. Because geologic conditions can significantly alter the amplitudes of seismic energy and can cause focusing and scattering energy, realistic time histories should include the effects of geologic conditions along the propagation path from the fault and at the site itself. Empirical Green's functions used to capture the effect of the free surface, attenuation, refractions, reflections and scattering due to heterogeneities along the propagation path. In addition to this, EGFs inherently include linear site response at the site where they are recorded. Considering the above mentions, it can be clearly say that empirical Green's function method is one of the simplest techniques for predicting ground motion including all the information about the propagation path between the EGF source and the recording site and this is the main advantage of the EGF approach.

If we consider that high frequency ground motions strongly effected by heterogeneity and Marmara Region shows not only strong lateral heterogeneity (Barış et al., 2005) also sharp lateral velocity variations consistently (Karabulut, 2003), calculated one dimensional velocity structure model that used for some of the high frequency ground motion simulation algorithm can be produced unrealistic results. In this study, we demonstrate that empirical Green's functions successfully represent the heterogenic velocity structures and complex geological conditions of Marmara region. Considering that small magnitude earthquakes used as EGFs include all of the geological effect in three dimensions along the propagation path, it is easily understand that EGF method based on representation theorem developed by Hutchings and Wu (1990) and Hutchings (1991) is powerful method to produce realistic ground motion simulations.

2. DATA

The data set composes of one main event (Mw=5.0) and its aftershock (Mw=3.6) were occurred Central Marmara Fault (CMF) that is main extension of northern branch of NAFZ in the Marmara sea (Figure 2). This data set recorded by broadband seismometer network operated by Boğaziçi University Kandilli Observatory and Earthquake Research Institute (BU-KOERI). Focal mechanism solutions were calculated using by first arrival of P waves. Table 1 lists origin time and hypocenter of the events reported by BU-KOERI. The names and locations of stations used in this study are shown in figure 2 and are listed in Table 2.

Table 1. Simulated main event and Empirical Green's function.

EQ ID	Date	Lat (N)	Long (E)	Depth	Mw	Location
E01	25.07.11 17:57	40.811	27.739	15.3	5.0	CMF
G01	25.07.11 20:43	40.817	27.736	5.4	3.6	CMF

Table 2. Seismometer stations that we used to calculate source parameters of the events and to synthesize main earthquakes.

ST ID	Location	Latitude (N) (Deg)	Longitude (E) (Deg)	Elevation (m)	Type
ARMT	ARMUTLU	40.5683	28.8660	320	3ESP-DM24
CRLT	ÇORLU	41.1290	27.7360	230	3ESP-DM24
CTYL	ÇATALCA	41.4760	28.2897	77	3T-DM24
EDC	EDİNCİK	40.3468	27.8633	257	3T-DM24
MRMT	MARMARA ADASI	40.6058	27.5837	213	3T-DM24

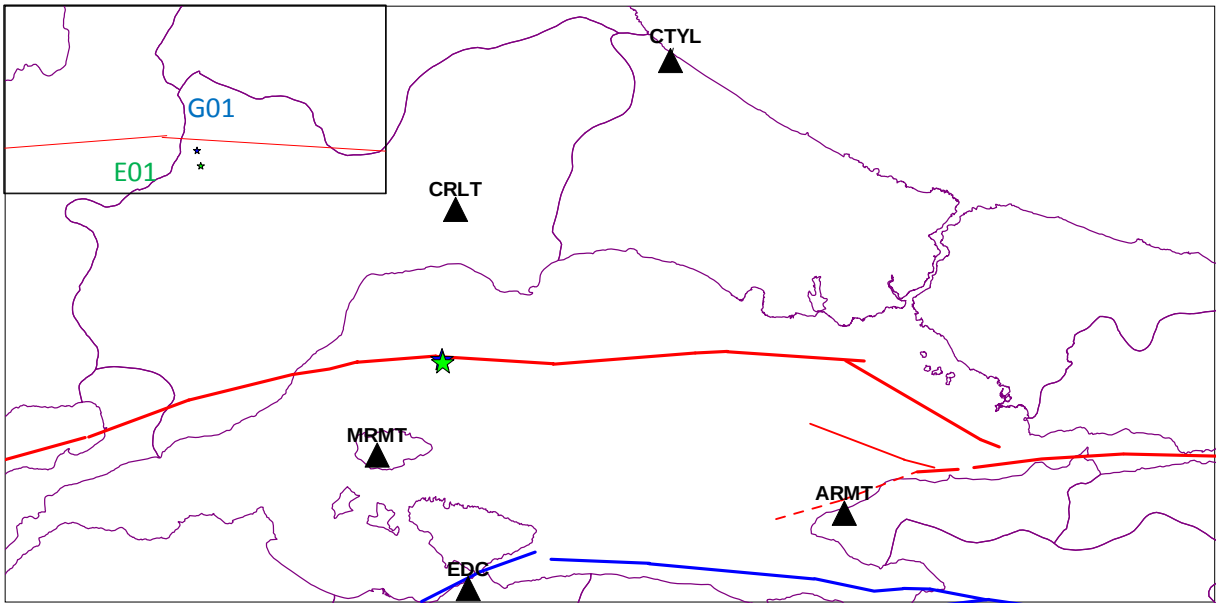

Figure 2. Simulated earthquake (Green star) and its aftershock (Blue star) together with broadband recording system.

3. DETERMINATION OF SOURCE PARAMETERS

We used computer program NetMoment (Hutchings, 2004) to estimate source parameters of the main earthquake and its aftershock. It conducts a simultaneous inversion to obtain moment (M_o), source corner frequency (f_c) and site specific attenuation (t^*_g). Simultaneous inversion is based upon the assumption that corrected long period spectral levels and the source corner frequencies from a particular earthquake will have the same value at each site so that, differences in spectra can be attributed to propagation path, individual site attenuation and site response. We corrected spectra for whole path attenuation (t^*_r) and solved for site specific attenuation (t^*_g). Because, the whole path attenuation (t^*_r) can be differ at each site in the highly heterogeneous Marmara region this inversion may lead to bias in corner frequency. Even though NetMoment can remove site response from the calculation if it is known generally, we prefer to include only those sites that do not have site amplification. We do not take into account amplification function due to site response during analysis and this may also cause some of the scatter in the results.

We used a nonlinear least squares best fit of displacement spectra of the S-wave energy of the recorded seismograms to the Brune source model to solve for our free parameters. The Fourier amplitude spectra of recorded seismograms were corrected to represent moment at the long period asymptote and for whole path attenuation. They were then fit to the Brune (1971) displacement spectral shape with site specific attenuation (t^*_g) and moment as the long period spectral asymptote. Spectra were fit to the modified Brune spectra:

$$\Omega(f) = \frac{M_o \exp\left(-\pi f t_g^*\right)}{\left[1 + \left(\frac{f}{f_c}\right)^2\right]} \qquad (3.1)$$

Where M_o is the moment, f is frequency, f_c is the source corner frequency and t^*_g is site specific attenuation. The best fitting combination of free permeates (M_o, f_c, t^*_g) was found by iteration from a starting model using the Simplex algorithm. The correction to spectra prior to the joint inversion is based upon the equation for moment from Aki and Richards (1980, pg. 116). Spectra of recorded seismograms were corrected by:

$$\Omega'(f)_i = \frac{4\pi R^{\alpha} \rho_x^{1/2} \rho_\zeta^{1/2} \beta_x^{1/2} \beta_\zeta^{5/2}}{S^S F^S} U(f) \exp\left(-\pi f t_r^*\right) \tag{3.2}$$

where *U(f)* is the recorded displacement spectra, t_r* is whole path attenuation, R^{α} is correction for geometrical spreading factor where α=1.0 for distances less than 100 km and 0.5 greater distances, ρ_x is density at the station and , ρ_ζ is density at the source. We used the P wave velocity to obtain density (ρ) values following Lama and Vutukuri (1978). β_x is shear velocity at the station and β_ζ is shear velocity at the source. S and F are the free surface correction and focal mechanism correction, respectively. The free surface correction factor is determined from the one dimensional velocity model using the reflection coefficients as outlined in Aki and Richards (1980, pg. 190). The focal mechanism correction is determined by the radiation pattern as outlined by Aki and Richards (1980, pg. 115).

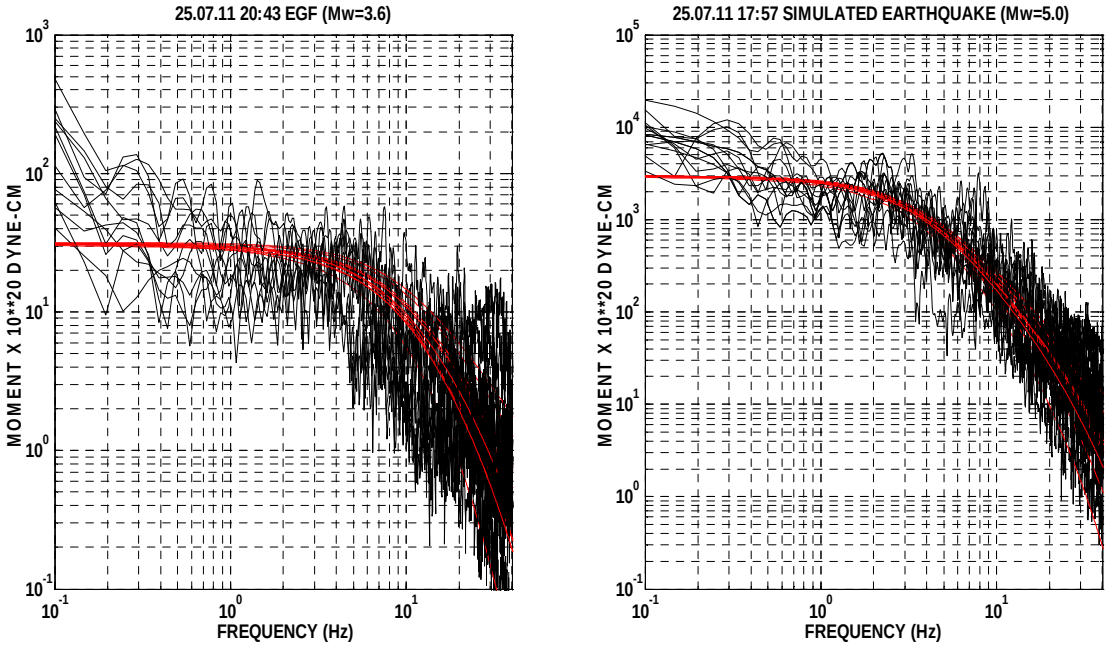

Figure 3. Corrected spectra of all recordings for 25.07.2011 17:57 (Mw=5.0) simulated event and 25.07.2011 20:43 (Mw=3.6) EGF. Corrected spectra from each station (black lines) are fitted to Brune spectra (red lines).

Before applying the inversion NetMoment analyzes the data's Signal to Noise Ratio (SNR). Because of this, frequency range for each individual fit is different for each station. In this study ten seconds of direct S wave arrivals were used and signal to noise ratio was selected 10. Corrected spectras were fit to equation 1 by fitting frequencies from 0.5 Hz to 25 Hz for aftershock and main event. Figure 3 shows how we fit spectra simultaneously for source, site and path attenuation. The differences in shapes of individual spectra are due to site specific (t^*_g). The solid line shows the modified Brune model over the frequency band that we used. Actual moment is the projection of this fit to asymptotic low frequency. Table 3 lists the source parameters determined for the main event and event that we used as an empirical Green's function.

Table 3. Calculated source parameters for the main events and events that we used as a Green's functions

EQ ID	Mechanism Stk Dip Rake	Mw	M_0	f_c
E01	346 50 -11	5.0	0.303±0.062E+24	1.7
G01	130 47 -75	3.6	0.322±0.114E+22	5.0

4. IMPLEMENTING EARTHQUAKE SYNTHESIZED METHODOLOGY

To develop realistic synthetic ground motions for specific sites, we used computer program Empsyn which calculates synthetic seismograms by numerically computing the discretized representation relation with empirical Green's functions. To model all kinds of effects, we synthesize ground motion with physics based solutions of earthquake rupture that utilize empirical Green's functions and apply physically based rupture parameters. By physically based we refer to ground motion syntheses derived from physics and understanding of the earthquake process (Hutchings et al., 2007).We used an exact solution to the representation relation for finite rupture that utilizes empirical Green's functions (Hutchings and Wu, 1990). Here, we use recordings of small earthquakes to provide empirical Green's functions for frequencies 0.5 to 20 Hz.

Empirical Green's functions are defined as recordings of effectively impulsive point source events (Hutchings and Wu, 1990) and their stress drop changes are reflected only in the differences of their seismic moment. 'Effectively impulsive point source' refers to the observation that factors such as rise time, rupture duration or source dimension are small enough that their effect can not be observed in the frequency band of interest (Hutchings et al., 2007). The empirical Green's functions have a accuracy at high frequencies, their displacement source spectra is flat up to the highest frequency of interest, and scale linearly for differences in seismic moments. They include the actual effects of velocity structure, attenuation and geometrical spreading.

Empirical Green's functions can be combined with synthetic slip functions and summed to synthesize an extended source earthquake. Because their source events have spatial extent, they can be summed to simulate fault rupture without loss of information, thereby potentially exactly computing the representation relation.

The discretized representation relation can be written as:

$$u_n(X,t) = \sum_{i=1}^{N} \frac{\mu_i A_i S(t')_i}{M^e_{0\,i}} * e_n\left(X, t'-t_r\right)_i \tag{4.1}$$

This is the equation that computer program EMPSYN which calculates synthetic seismograms is used. That is exact solution for the representation relation under certain conditions and it is our intent to keep as close to the mathematically exact solution as possible, with approximations adding to the uncertainty of the solution. In this equation (X,t) are position and time in space relative to the hypocenter and origin time of the synthesized earthquake. *N* is number of elements and *i* refers to values at an element. A_i is an elemental area such that $\sum A_i$ equals the total rupture area. $S(t')_i$ is the desired slip function at an element analytically deconvolved with the step function. $e_n\left(X, t'\right)_i$ empirical Green's function for the i^{th} element obtained from recordings of small earthquake with effectively a step source time function and interpolated to have a source and origin time at the location of the i^{th} element. t' is relative to the origin time of the source event corrected for element location. t_r is the rupture time from the hypocenter to the element, which is the integral of radial distance from the hypocenter of the synthesized earthquake divided by the rupture velocity, which can be a function of position on the fault. μ_i is the rigidity at an element, $M^e_{0\,i}$ is the scalar seismic moment of the source event, and * is the convolution operator. U_n has the same units as e_n.

5. SYNTHETIC RUPTURE MODELS FOR SIMULATED EARTHQUAKE

Our earthquake rupture models rely on moment, slip vector, fault geometry, hypocenter, rupture velocity, healing velocity, rupture roughness, rise time and stress drop. The fault rupture surface area was discretized into 0.01km^2 elemental areas, which are small enough that modeled rupture is

continuous for frequencies f≤20 Hz. The rupture initiates at the hypocenter and propagates radially at some fraction of the shear wave velocity. We used the Kastrov slip function to calculate the slip at a point; we approximate the shape as a ramp. Rupture velocity is selected 0.9 times the shear wave velocity and Healing velocity is selected between 0.85 times the rupture velocity considering that Rayleigh and shear wave velocities. The healing velocity is the velocity for the stress pulse that terminates slip and it is initiated after the rupture arrives at any fault edge. Healing velocity controls the rise time that is equal to time it takes, after the initiation of rupture, for the first healing phase to arrive. In other words, it is the shortest time for the rupture front to reach an edge and travel to a point at the healing velocity. Fault rupture geometry is constrained to be rectangular. The rupture area was selected 2.1 km^2. Strike, rake, dip are selected based on focal mechanism solutions and considering geometrical spreading of NAFZ segments in the vicinity of Marmara Sea. Roughness is simulated as elements resisting rupture and then breaking. A percentage of elements (33%) have a shortened rise times between 0.1 and 0.9 times the original value or those of neighboring elements, but with rupture completed at the same time. This will distribute randomly on the fault because of the radial arrangement of elements. These rough elements have corresponding high stress drop. Stress drop is a dependent variable derived from the Kostrov slip function and allowed to vary due to two other effects modeled in rupture. The first, asperities are allowed to have different stress drop than surrounding portions of the fault. Second stress drop is constrained to diminish near the surface of the earth. In this study, because simulated earthquakes are mid-sized earthquakes, we do not use asperities and rupture never reach to the surface.

6. RESULTS

Using the data set that include one EGF and one target event, synthesized ground motion time histories are calculated and compared with real earthquake records in terms of time history waveforms and Fourier spectrum. Simulated and real time histories and spectrums for two horizontal components are provided for five recording stations. in Figures 4 and 5 respectively.

The distance between target event and EGF is 0.73 km. The closest distance between recording stations to target earthquake is 26.5 km (MRMT) and the most distant station is 99 km (ARMT). Other stations distances are 35 km (CRLT), 53.5 km (EDC) and 86.5 km (CTYL) respectively. Considering the arrival time of the P and S waves, the duration of the records and the shape of the observed and synthesized records it is obvious that a good similarity in time domain for the five different stations is achieved (Figure 4). For some of the stations (CRLT, EDC, ARMT) observed absolute amplitudes of the real and the synthesized records match perfectly, for some other stations (MRMT, CTYL) the consistency is not perfect but acceptable. The reason of the amplitude differences between real and synthesized records can be related to error in moment calculations. In frequency domain (Figure 5) energy content of real and synthesized records for two horizontal components are matched very well in the frequency range of 0.5 to 20 Hz except MRMT station. For this station real and simulated spectrums are matched only in the frequency range of 0.5 to 2 Hz.

7. CONCLUSIONS

Modeling exact waveforms was not perfect for all of the stations. However, a good match to observed seismograms was obtained for frequency content, absolute amplitudes and energy distribution. It is clear that nobody expect simulated time history obtained from a simple source model and one EGF to match each cycle of the real earthquake record. Also the same thing can be say that the energy content of simulated and real event do not match for all frequencies in the spectrum. Considering that main purpose of the methodology is to produce meaningful results in engineering point of view and not for exact computations of waveforms, it can be clearly say that the EGF summation approach by Hutchings and Wu (1990) is feasible and practical method for simulating ground motion for midsized earthquakes in highly heterogeneous Marmara region.

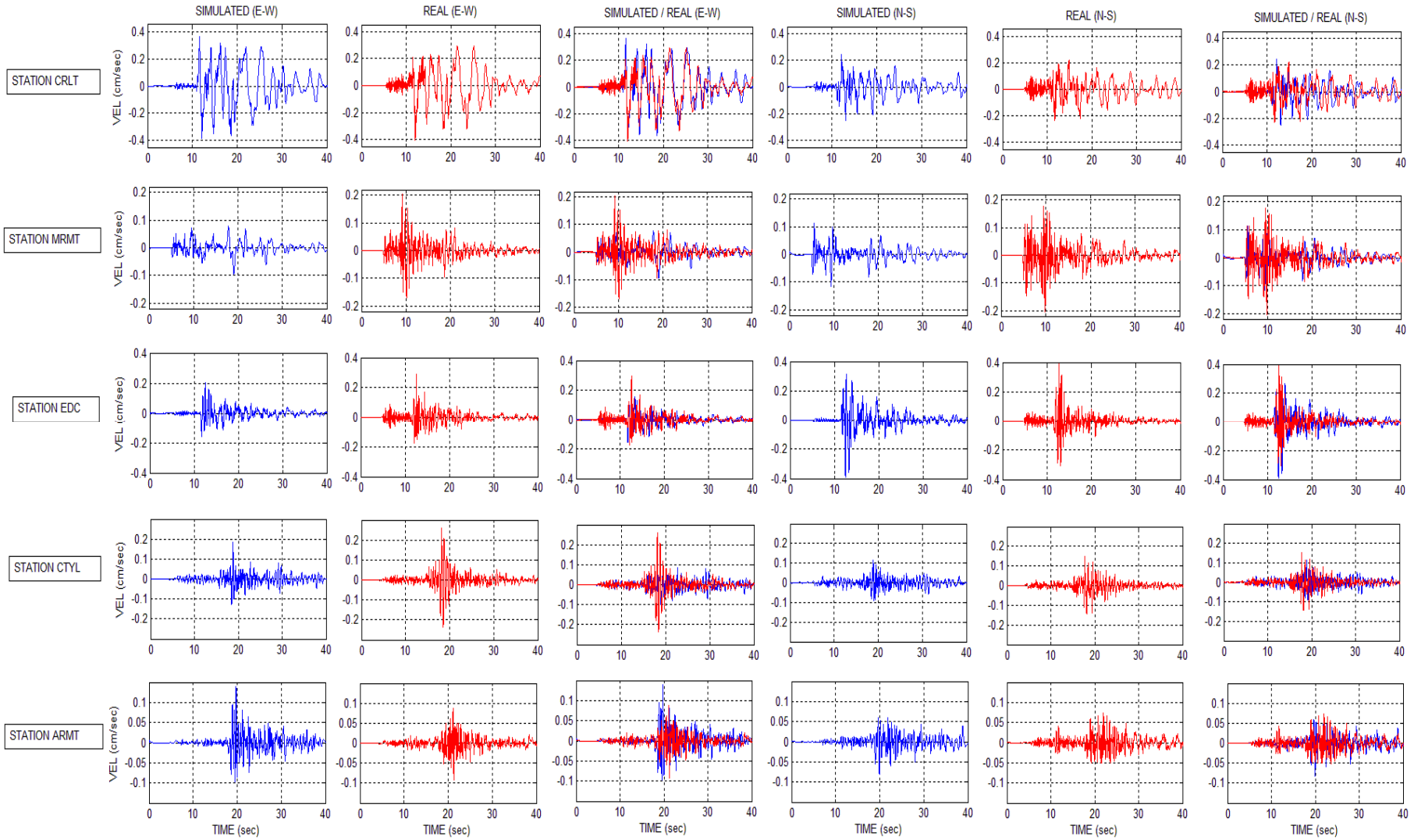

Figure 4. Real and Simulated time history records for Central Marmara Earthquake (M_w=5.0).

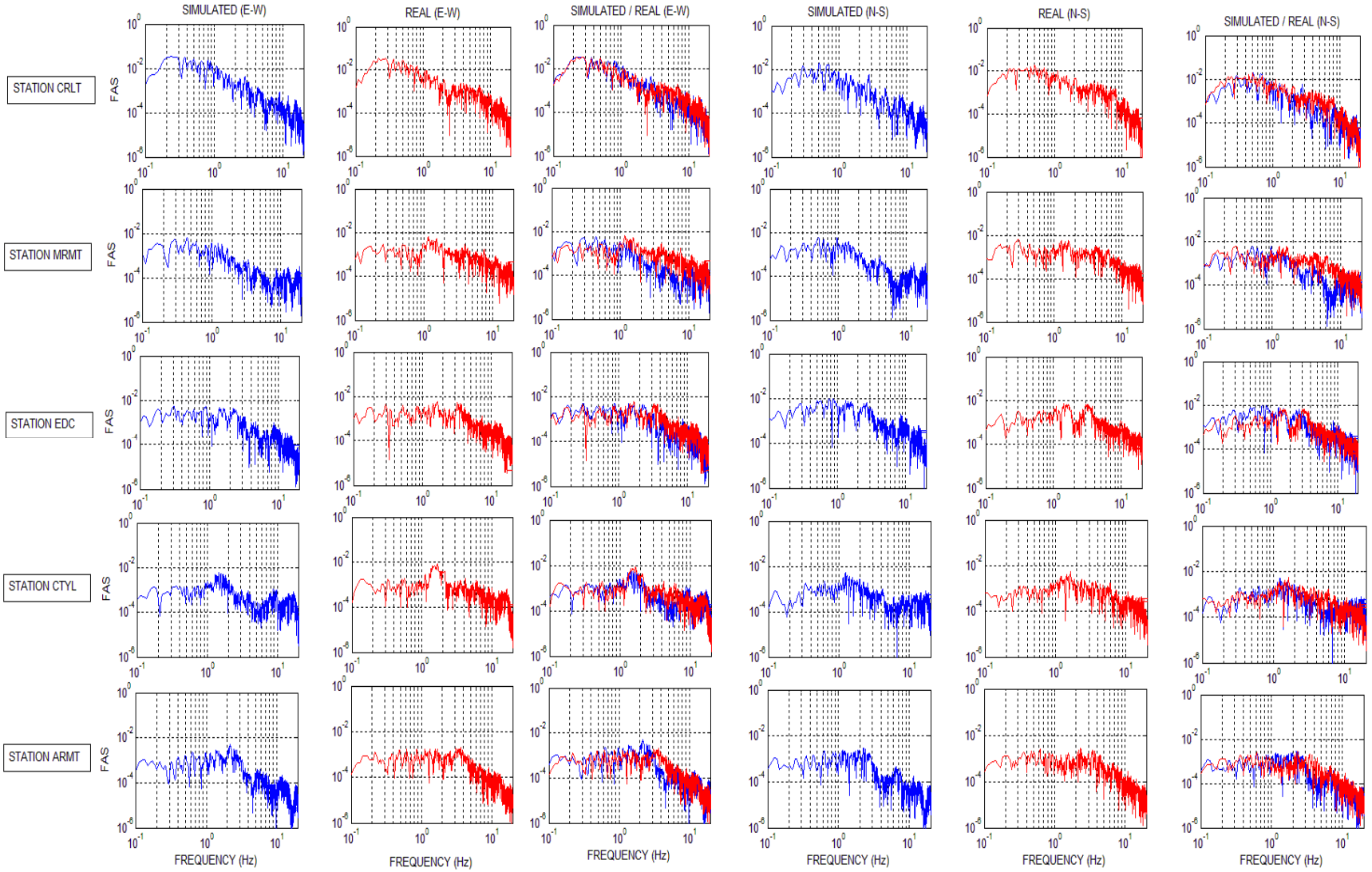

Figure 5. Real and Simulated Fourier Amplitude Spectrum for Central Marmara Earthquake (M_w=5.0).

ACKNOWLEDGMENT
This work was supported by the Scientific and Technological Research Council of Turkey (TÜBİTAK-MAG) under Project Number 108M584 and Scientific Research Projects Coordination Unit of Istanbul University under Project number 1827.

REFERENCE

Aki, K. and P. G. Richards, (1980). Quantitative seismology,Theory and Methods, VolumesI and II, W. H. Freeman and Company, San Francisco, CA

Ansal, A., Akıncı, A., Cultera, C., Erdik, M., Pessina, V., Tönük, G., Ameri, G., (2009). Loss Estimation in Istanbul based on deterministic scenarios of the Marmara Sea region (Turkey). Soil Dynamics and Earthquake Engineering. 29:4,699-709.

Armijo, T., Meyer, B., Navarro, S., King, G., Barka, A., (2002). Asymmetric slip partitioning in the Sea of Marmara pull-apart: a clue to propagation processes of the North Anatolian Fault. Terra Nova, 14:80–86.

Atakan, K., Ojeda, A., Meghraoui, M., Barka, A., Erdik, M., Bodare, A., (2002). Seismic hazard in Istanbul following the 17 August 1999 Izmit and 12 November 1999 Duzce earthquakes. Bul. Seis. Soc. Am., 92,466-482

Barış, S., Nakajima, J., Hasegawa, A., Honkura, Y., Ito, A., Ucer, B., (2005). Three dimensional structure of Vp, Vs and Vp/Vs in the upper crust of the Marmara Region, NW Turkey. Earth Planets Space, 57,1019-1038.

Barka AA, Kadinsky-Cade K (1988). Strike-slip fault geometry in Turkey and its influence on earthquake activity. Tectonics 7: 663-684

Brune, J.N.,(1971). Tectonic stress and the spectra of seismic shear waves from earthquakes, J. Geophys. Res.,75, 4997–5010, (Correction, J. Geophys. Res. 76 (20), 5002, 1971)

Erdik M, Demircioglu M, Sesetyan K, Durukal E, Siyahi B., (2004). Earthquake hazard in Marmara region, Turkey. Soil Dynamics and Earthquake Engineering 24:605–31.

Gökaşan, E., Ustaömer, T., Gazioğlu, C., Yücel, Z.Y., Öztürk, K., Tur, H., (2003). Morpho-tectonic evolution of the Marmara Sea inferred from multi-beam bathymetric and seismic data, Geo-Mar Lett, 23:19–33.

Hutchings, L., Wu, F (1990). Emprical Green functions from small earthquakes. A waveform study of locally recorded afterschoks of the San Fernando earthquake. J. Geophys. Res., 95, 1187-1214.

Hutchings, L. (1991). Prediction" of strong ground motion for the 1989 Loma Prieta earthquake using empirical Green's functions. Bull. Seismol. Soc. Am. 81, 88–121

Hutchings, L., (2004). Program NetMoment, a Simultaneous Inversion for Moment, Source Corner Frequency, and Site Specific t*, Lawrence Livermore National Laboratory, Livermore, CA, UCRL-ID 135693.

Hutchings, L., Ioannidou, E., Kalogeras, I., Voulgaris, N., Savy, J., Foxall,W., Scognamiglio, L., Stavrakakis, G., (2007). A physically-based strong ground-motion prediction methodology; application to PSHAand the 1999M=6.0 Athens earthquake. Geophys. J. Int., 168,569–680.

Karabulut H., Özalaybey S., Taymaz T., Aktar M., selvi O., Kocaoğlu A., (2003). A Tomographic image of the shallow crustal structure in The Eastern Marmara, Geophys. Res. Lett., 30:24.

Lama, R.D. and Vutukuri, V.S., (1978). Handbook on Mechanical Properties of Rocks, Volume II: Testing Techniques and Results, Trans Tech. Publications, 1978, 245 pp., J. Phys. Earth. 42, 377–397.

Mathilde, B., Pulido, N., Atakan, K., (2007). Sensitivity of ground motion simulations to earthquake source parameters: A case study for Istanbul, Turkey. Bul. Seis. Soc. Am., 97:3,881-900

Parsons, T., (2004). Recalculated probability of M 7 earthquakes beneath the Sea of Marmara Turkey, J Geophys Res, 109:B05304.

Pulido N, Ojeda A, Atakan K, Kubo T., (2004). Strong ground motion estimation in the Sea of Marmara region (Turkey) based on a scenario earthquake. Tectonophysics, 391:357–74.

Pinar, A., Kuge, K., Honkura, Y., (2003). Moment inversion of recent small to moderate sized earthquakes: implications for seismic hazard and active tectonics beneath the Sea of Marmara, *Geophys J Int*, 153,133–145.

Şengör, A.M.C., Tüysüz, O., Imren, C., Sakinç, M., Eyidoğan, H., Görür, N., (2005). The North Anatolian Fault: a new look. Annu Rev Earth Planet Sci, 33:37–112.

Toksöz, M.N., Relinger R.E., Doll, C.G., Barka, A.A., Yalçin, N., (1999). Izmit (Turkey) earthquake of 17 August 1999: first report, Seismol Res Lett, 70:669–679.

Yilmaz Y, Gökaşan E, Erbay AA., (2009). Morphotectonic development of the Marmara Region. Tectonophysics doi:10.1016/j.tecto.2009.05.012